THE JOURNAL OF PHYSICAL CHEMISTRY A
A JOURNAL OF THE AMERICAN CHEMICAL SOCIETY

pubs.acs.org/JPCA

Article

Significantly Accelerated Hydroxyl Radical Generation by Fe(III)−Oxalate Photochemistry in Aerosol Droplets

Published as part of The Journal of Physical Chemistry virtual special issue "Michael R. Hoffmann Festschrift".

Longqian Wang,[▽] Kejian Li,[▽] Yangyang Liu, Kedong Gong, Juan Liu, Jianpeng Ao, Qiuyue Ge, Wei Wang, Minbiao Ji, and Liwu Zhang*

Cite This: *J. Phys. Chem. A* 2023, 127, 250−260

Read Online

ACCESS | Metrics & More | Article Recommendations | Supporting Information

ABSTRACT: Fe(III)−oxalate complexes are ubiquitous in atmospheric environments, which can release reactive oxygen species (ROS) such as H_2O_2, $O^{\bullet 2-}$, and $OH^{\bullet}$ under light irradiation. Although Fe(III)−oxalate photochemistry has been investigated extensively, the understanding of its involvement in authentic atmospheric environments such as aerosol droplets is far from enough, since the current available knowledge has mainly been obtained in bulk-phase studies. Here, we find that the production of $OH^{\bullet}$ by Fe(III)−oxalate in aerosol microdroplets is about 10-fold greater than that of its bulk-phase counterpart. In addition, in the presence of Fe(III)−oxalate complexes, the rate of photo-oxidation from SO_2 to sulfate in microdroplets was about 19-fold faster than that in the bulk phase. The availability of efficient reactants and mass transfer due to droplet effects made dominant contributions to the accelerated $OH^{\bullet}$ and SO_4^{2-} formation. This work highlights the necessary consideration of droplet effects in atmospheric laboratory studies and model simulations.

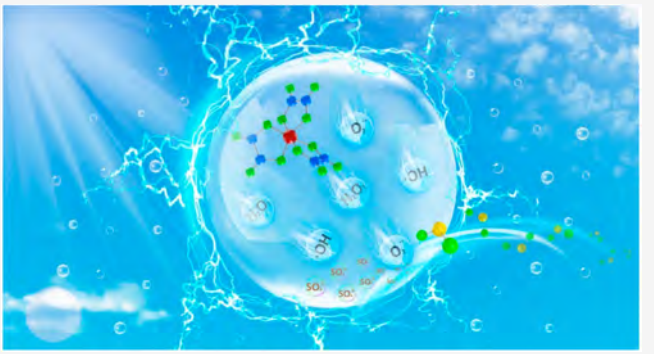

Downloaded via FUDAN UNIV on February 28, 2023 at 23:27:12 (UTC).
See https://pubs.acs.org/sharingguidelines for options on how to legitimately share published articles.

1. INTRODUCTION

Atmospheric aerosols play a crucial role in affecting global climate by absorbing sunlight and modifying cloud characteristics.[1,2] Nevertheless, an evident gap between ground-based observations and numerical modeling still remains.[3−5] For instance, the oxidation of volatile organic compounds (VOCs) is one of the major contributors to the amount of secondary organic aerosols (SOAs) in the atmosphere, but great prediction uncertainties for the two constituents are inevitable due to unknown atmospheric processes, e.g. a different aging process where VOCs are transformed to SOA in the presence of oxidants. This hinders a precise evaluation of the response of climate change to the aerosol constituents.[6,7] As a consequence, further exploration of the missing reaction channel of great oxidation potential is essentially important to improve the accuracy of modeling predictions of climate change.

Iron is one of the most abundant transition metals in nature and can strongly combine with organic ligands to form complexes.[8] Oxalic acid and the corresponding salts are the most common dicarboxylic acids in the troposphere.[9] Over the past few decades, Fe(III)−oxalate complexes have been widely studied as representatives of Fe(III)−dicarboxylate complexes.[10,11] The Fe(III)−oxalate chelates can undergo photo-Fenton reactions in aquatic and atmospheric environments. As shown in chemical reactions R1−R6, the ligand-to-metal charge transfer and redox cycle of Fe(II)/Fe(III) can lead to the formation of reactive oxygen species (ROS) such as H_2O_2, $O_2^{\bullet -}$, and $OH^{\bullet}$,[12−14] which are of great significance for various atmospheric chemistry processes in both the aqueous phase and aerosol particles.[15] Therefore, the atmospheric photoreactions of Fe(III)−oxalate complexes deserve a great deal of attention.[16]

$$[Fe(III)(C_2O_4)_3]^{3-} + h\nu \rightarrow [Fe(II)(C_2O_4)_2]^{2-} + C_2O_4^{\bullet -} \quad (R1)$$

$$C_2O_4^{\bullet -} \rightarrow CO_2^{\bullet -} + CO_2 \quad (R2)$$

$$CO_2^{\bullet -} \rightarrow O_2 + CO_2 + O_2^{\bullet -} \quad (R3)$$

$$O_2^{\bullet -} + H^+ \leftrightarrow HO_2 \quad (R4)$$

Received: August 18, 2022
Revised: December 15, 2022
Published: January 3, 2023

© 2023 American Chemical Society

https://doi.org/10.1021/acs.jpca.2c05919
J. Phys. Chem. A 2023, 127, 250−260

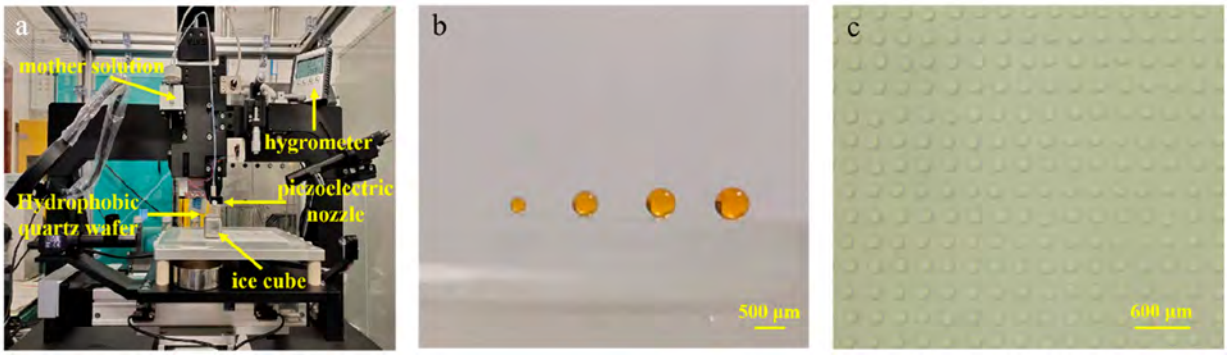

Figure 1. Setup for aerosol microdroplet generation. (a) Photo of the inkjet printer for microdroplet generation. (b) Profile photo of the printed microdroplets with different sizes. (c) Micrograph of the printed microdroplet array with a uniform diameter.

$$2HO_2^{\bullet} \leftrightarrow H_2O_2 + O_2 \quad \text{(R5)}$$

$$Fe(II) + H_2O_2 \leftrightarrow Fe(III) + OH^{\bullet} + OH^{-} \quad \text{(R6)}$$

At present, the reaction mechanisms and atmospheric environmental implications of Fe(III)−oxalate photochemistry have been investigated extensively; however, most of the studies were performed in bulk solution.[17−19] Noticeably, the authentic atmospheric reactions generally occurred in micrometer-sized compartments (e.g., aerosols, cloud and fog droplets), with sizes ranging from nanometers to hundreds of micrometers.[20] Inspired by nature, microdroplet chemistry has attracted substantial attention in recent years. Microdroplets have a remarkably different reaction environment and exhibit distinct physicochemical characteristics in comparison with their traditional bulk-phase counterpart.[21,22] It has been demonstrated that the chemical reactions in microdroplets could be dramatically accelerated compared to the same reactions in bulk solution.[23] Moreover, some thermodynamically unfavorable reactions can spontaneously occur in microdroplets without any external additives, such as H_2O_2 production,[24,25] the reduction of organics,[26] and ribonucleoside synthesis.[27,28]

Nevertheless, the photochemical reactions of Fe(III)−oxalate complexes in aerosol microdroplets have rarely been studied. In our previous work, we found that the photochemical oxidation of organic dyes was accelerated in an Fe(III)−oxalate microdroplet.[29] However, the production of $OH^{\bullet}$ and potential impacts on trace gas conversion in atmospheric aerosol droplets are not well-known. Wang et al. found that the photolysis rate of Fe(III)−oxalate in a droplet was almost two orders of magnitude faster than that in the bulk, which was ascribed to the intensified Fe(III)−oxalate photochemistry at the water−air interface of the droplet.[30] In addition, Thomas and co-workers investigated the Fe(III)−oxalate-mediated oxidation of glycolaldehyde in microliter droplets utilizing field-induced droplet ionization mass spectrometry (FIDI-MS) and found that the photodissociation of Fe(III)−oxalate can lead to the formation of volatile oxidation products in tropospheric aqueous aerosols.[31] Even though the photoreaction of Fe(III)−oxalate in atmospheric aerosols is not fully understood, its contribution to oxidation potential in the atmosphere might be underestimated.

Herein, the production of $OH^{\bullet}$ by Fe(III)−oxalate photochemistry in aerosol droplets under typical atmospheric environments was investigated and compared with that in the conventional bulk-phase reaction. The hydroxyl radical ($OH^{\bullet}$), with its strong oxidation capability, could significantly influence atmospheric chemistry processes such as the oxidation of organics, the transformation of trace gases, and even global climate change. The effects of the light irradiation intensity, the solution pH, the reactant concentration, and the aerosol droplet size are discussed in detail. Different from previous reports, an inkjet printer is employed to generate aerosol droplets with the desired size, which enables us to better study the size effects of aerosol microdroplets on atmospheric chemistry. Furthermore, SO_2 oxidation for ambient sulfate formation in the presence of Fe(III)−oxalate complexes in microdroplets was also studied. The experimental results show that $OH^{\bullet}$ generation and S(IV) oxidation in aerosol microdroplets were accelerated by dozens of times as compared to their bulk-solution counterparts. Potential reasons behind photoreaction acceleration in aerosol droplets were related to O_2 availability and the droplet effect. This work will provide a deep understanding and highlight the significance of aerosol microdroplets on atmospheric photochemistry.

2. EXPERIMENTAL SECTION

2.1. Microdroplet Generation and Photochemical Reactions. A typical Fe(III)−oxalate solution containing 500 μM $FeCl_3$ and 3.5 mM $Na_2C_2O_4$ was prepared for photochemical experiments. The ionic strength of this Fe(III)−oxalate solution was 8.25×10^{-3} mol kg^{-1}, which was calculated using eq 1, where c_i is the molality of ion i (mol kg^{-1}) and Z_i is the charge of the ion.

$$I = \frac{1}{2}(c_1Z_1^2 + c_2Z_2^2 + c_3Z_3^2 + ...) = \frac{1}{2}\Sigma c_iZ_i^2 \quad (1)$$

To quantitatively determine the $OH^{\bullet}$ concentration, 10 mM benzoic acid (BA) was added as a quencher of $OH^{\bullet}$.[32,33] Here, 1, 2 and 3 mM NaCl was first added into the Fe(III)−oxalate solution to eliminate the influence of Cl^- on $OH^{\bullet}$ production, as shown in Figure S1. There was almost no obvious variation of $OH^{\bullet}$ production in the presence of different NaCl concentrations, which suggested that the competition for $OH^{\bullet}$ between Cl^- and BA might be insignificant and that Cl^- did not cause interference in the $OH^{\bullet}$ determination. The initial solution pH was adjusted to 3.5 using 0.1 M HCl and 0.1 M NaOH. Both bulk-phase and microdroplet experiments were conducted to investigate the production of $OH^{\bullet}$ by Fe(III)−oxalate photochemistry. For the microdroplet photoreaction, a custom-designed reactor (as shown in Figure S2) was used to provide an enclosed high-humidity environment. Hundreds of microdroplets (around 200−300) with diameters

https://doi.org/10.1021/acs.jpca.2c05919
J. Phys. Chem. A 2023, 127, 250−260

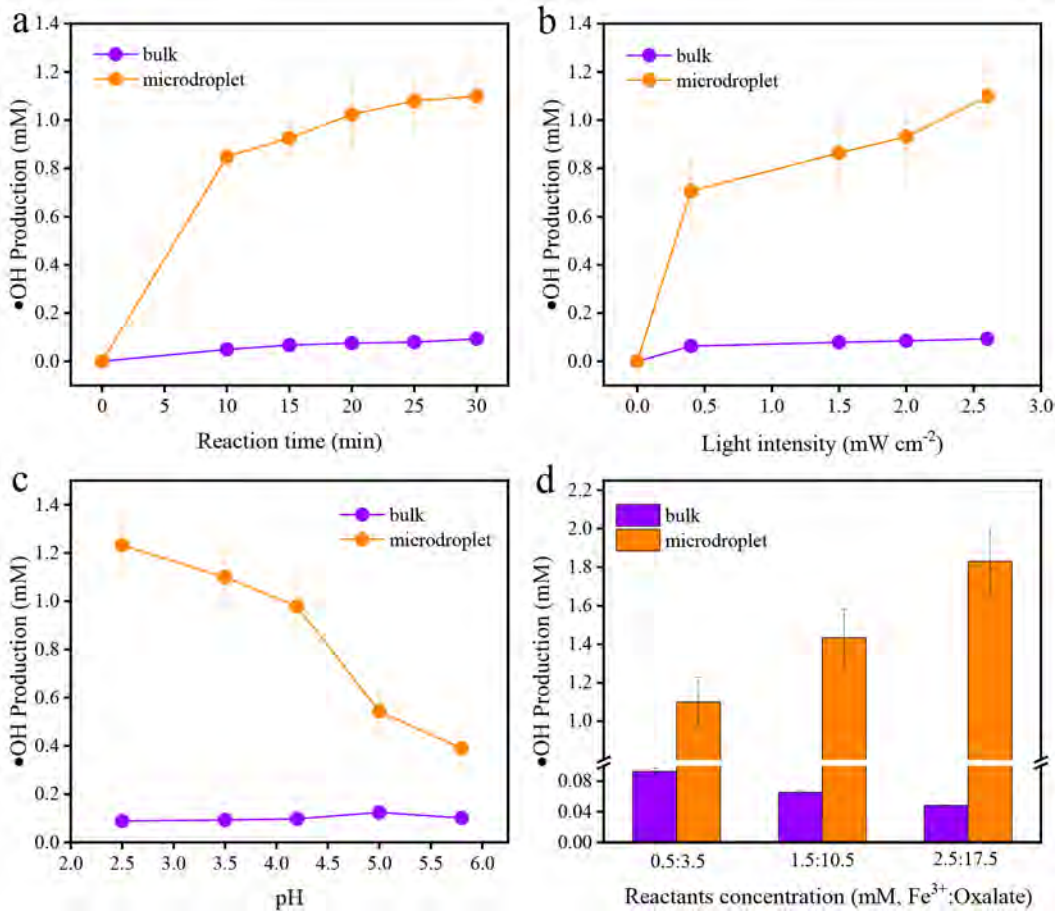

Figure 2. Hydroxyl radical generation by Fe(III)−oxalate complex photolysis in aerosol microdroplets and the bulk phase. (a) Influence of the light irradiation time. (b) Impact of the light irradiation intensity. (c) Effect of the solution pH. (d) Influence of the Fe(III)−oxalate concentration. Experimental conditions are as follows: [Fe(III)] = 500 μM, [oxalate] = 3.5 mM, pH 3.5, and reaction time of 30 min.

(Φ) mainly ranging from 100 to 500 μm (average diameter of 260 μm) were generated using a nebulizer and collected on a superhydrophobic quartz wafer (water contact angle of 144 ± 2°, see Figure S3). The water evaporation of the microdroplets is negligible during the reaction period, as shown in Figure S4, benefiting from our maintenance of high relative humidity (RH ∼ 93%) and room temperature in the reaction chamber. The bulk-phase reaction was performed in a miniature beaker with 10 mL of a Fe(III)−oxalate solution (thickness, ∼ 60 mm). The temperature during the photoreaction was kept at 25 ± 2 °C by an electric fan. After light irradiation (365 nm UV lamp, ∼ 2.6 mW cm^{-2}), the microdroplets were collected with a coverslip.[34] Then, a specific amount of the collected solution was taken by a pipet, diluted quantitatively using 0.1 M HCl, and filtered through a 0.22 μm PTFE membrane filter for further analyses. All the chemicals used are listed in section S1.

To study the effects of microdroplet size on the production of $OH^{\bullet}$, an array of microdroplets with a specific size was generated by an inkjet printing device (supplied by jetlab II, MicroFab) consisting of four modules: a piezoelectric nozzle with diameter of 40 μm, a high-speed drop-watch camera system, a three-axis movement platform, and a pressure control system connected to the air compression pump (as shown in Figure 1a). A succession of two sine pulses (consecutively positive/negative) was chosen as the bipolar control waveform for microdroplet printing with a voltage of 28 V, a period time of 96 μs, and a printing frequency of 300 Hz. The distance between the nozzle and the hydrophobic substrate was ∼1.5 mm. Noticeably, a stainless-steel ice cube was placed under the hydrophobic substrate to inhibit the volatilization of microdroplets during printing. Figure 1b shows the microdroplets with different sizes generated by the inkjet printing device on a superhydrophobic quartz wafer. It is worth noting that hardly any $OH^{\bullet}$ was generated in the freshly printed microdroplets from the solution containing Fe(III)−oxalate or without light irradiation, which might be because that the microdroplet size was comparatively large in comparison with the previous study.[35] The results indicate that the detected $OH^{\bullet}$ in the study was produced from Fe(III)−oxalate photolysis.

2.2. Oxidation of SO_2 by Fe(III)−Oxalate Photochemistry. Furthermore, SO_2 oxidation by Fe(III)−oxalate complexes in microdroplets was conducted to show the effects of aerosol microdroplet on atmospheric chemistry following the procedures for $OH^{\bullet}$ production investigation, and the bulk-phase experiment was performed in a quartz reactor with gas inlet and outlet. The gas flow rate and SO_2 concentration (100 and 1 ppm, respectively) were controlled by employing mass flow controllers. The high-humidity air was obtained by passing fresh air through a bottle filled with ultrapure water. For the bulk-phase reaction carried out under magnetic stirring, the mixed gases were first bubbled into the solution for 15 min prior to light irradiation and then continuously purged during the photoreactions. For the microdroplet system, the mixed gases with a high RH that contained SO_2

https://doi.org/10.1021/acs.jpca.2c05919
J. Phys. Chem. A 2023, 127, 250−260

and air were purged into the headspace of a custom-designed reactor for 15 min, then purging was stopped and the reactor was sealed before light irradiation. The experimental setups for sulfate formation in microdroplets and the bulk solution are shown in Figure S5. In addition, the control experiments were conducted under dark conditions. The samples were withdrawn at given time interval, and 1.5 mL of 5 vol % isopropanol (IPA) was used to prevent further oxidation of S(IV). Then, the sample was filtered through a 0.22 μm PTFE membrane filter for ion chromatographic identification.

2.3. Stimulated Raman Spectroscopy Measurements. SRS measurements were conducted in a homemade environmental chamber consisting of two coverslips (thickness of 0.14−0.17 mm) and a slide with a central perforation (thickness of ∼0.5 mm, hole diameter of 15 mm). The microdroplets generated from the Fe(III)−oxalate solution (concentrations of 0.1 M $FeCl_3$ and 0.5 M $Na_2C_2O_4$) were sprayed on a superhydrophobic quartz wafer using a nebulizer, then the microdroplets were sealed in the homemade chamber. We performed SRS spectroscopic characterization for microdroplets after 10 min of stabilization. The detailed steps of SRS measurements are shown in section S2.

2.4. Analytical Methods. The oxidation of benzoic acid (BA) to *p*-hydroxybenzoic acid (*p*-HBA) was used as a probe reaction to quantify $OH^•$ production. The *p*-HBA concentration was measured by high performance liquid chromatography (HPLC, LC-10AD) on a system equipped with an SPD-15C UV−vis detector and a WondaCract ODS-2 chromatographic column (250 mm × 4.6 mm × 5 μm). The mobile phase was a mixture of acetonitrile and 0.1 vol % H_3PO_4 (40:60 v/v) at a flow rate of 1 mL min^{-1}, and the detection wavelength was 256 nm. The calculation equation for the cumulative $OH^•$ concentration ($[OH^•]$) is shown in eq 2,[32] where [*p*-HBA] is the concentration of the detected *p*-HBA. The conversion factor (5.87) was obtained by intercalibration with the methanol probe using a pure $OH^•$ source (H_2O_2) and is in excellent agreement with *G* value data (∼6) for products formed from the reaction of benzoic acid with $OH^•$.[36] The calibration curve was established using standard samples with gradient concentrations (Figure S6).

$$[OH^•] = [p\text{-HBA}] \times 5.87 \quad (2)$$

The concentration of sulfate ions generated from SO_2 oxidation was detected using a Metrohm 883 Basic ion chromatograph. A weak-base eluent (3.2 mM Na_2CO_3 and 1.0 mM $NaHCO_3$) was used for analysis at a flow rate of 0.70 mL min^{-1}.

3. RESULTS AND DISCUSSION

3.1. Hydroxyl Radical Production by Fe(III)−Oxalate Photochemistry in Aerosol Microdroplets and the Bulk Phase. $OH^•$ plays a significant role in atmospheric oxidation processes and has direct and indirect effects on atmospheric chemistry and the global climate; therefore, $OH^•$ generation from photo-Fenton processes in atmospheric water droplets is of great significance. With this consideration in mind, we used the ubiquitous Fe(III)−oxalate chelates with noteworthy photoactivities in the atmospheric aqueous phase to investigate $OH^•$ production. Figure 2a shows the variation trend in the concentration of $OH^•$ produced by Fe(III)−oxalate complexes photolysis as a function of the irradiation time. Figure S7 shows the enlarged versions of $OH^•$ production in the bulk phase to give a clearer description. It is clear that the $OH^•$ production in both microdroplets and the bulk phase increased with time. Meanwhile, the yield of $OH^•$ in the microdroplets was about dozens of times higher than that in the bulk phase, indicating that the aerosol droplet environment can significantly accelerate $OH^•$ production from the photolysis of Fe(III)−oxalate complexes. Notably, the concentration of $OH^•$ in the microdroplets sharply reached 0.82 mM within first 10 min of irradiation and then slowly increased to 1.01 mM within another 20 min of reaction. The lower $OH^•$ production rates might be because the fast photo-Fenton reactions of Fe(III)−oxalate complexes in microdroplets resulted in the rapid consumption of H^+ and an increase in the pH, which would hinder the further photoreaction (discussed in detail below). In contrast, $OH^•$ production in the bulk phase gradually increased to only 0.09 mM at the end of the reaction with an almost constant rate, which might be because the reaction rate in the bulk phase was sluggish and the H^+ concentration was sufficient during the entire reaction process. The results further suggest that the photochemistry of Fe(III)−oxalate chelates can be promoted in aerosol droplets compared to their conventional bulk-phase counterpart.

The solar radiation intensity is affected by season, time of day, weather conditions, and geographic position, which would inevitably influence the efficiency of atmospheric photochemistry processes.[37] Therefore, the effects of the light illumination intensity on $OH^•$ generation were further investigated. As shown in Figure 2b, the concentration of $OH^•$ in the microdroplets reached 0.71 mM at a light intensity of 0.4 mW cm^{-2} and then continuously increased to 1.01 mM as the power density increased to 2.6 mW cm^{-2}. In sharp contrast, in the bulk-phase reaction, the concentration of $OH^•$ first increased to 0.09 mM (0.4 mW cm^{-2}) and then almost leveled off as the light intensity increased, which might be because of the low O_2 accessibility and competition reactions in the bulk-phase system.[38,39] Under the same illumination intensity, the production of $OH^•$ in microdroplets was one order of magnitude higher than that in the bulk phase, which showed that the Fe(III)−oxalate complexes in microdroplets could generate $OH^•$ more efficiently.

Aerosols, fogs, and cloud droplets throughout the atmosphere have been observed to exhibit pH values in the range of 2−6,[40] which would influence the atmospheric chemistry processes. Therefore, in this work, we adjusted the solution pH to investigate the related effects on $OH^•$ production by Fe(III)−oxalate photochemistry in both the bulk phase and microdroplets. As shown in Figure 2c, the $OH^•$ production in microdroplets decreased as the pH value increased but which was obviously higher than that in the bulk phase. Thus, the photo-oxidation ability of Fe(III)−oxalate complexes in atmospheric droplets was underestimated in most of the previous studies. The variation trend of $OH^•$ production in the bulk phase was first upward and then downward as the pH changed from 2.8 to 5.8. The disproportionation of $HO_2•$ and $O_2^{•-}$ for $OH^•$ production is strongly pH-dependent.[41] At low pH, $HO_2•$ is the dominant species and can react with Fe(II) to form H_2O_2 for $OH^•$ production, which is two orders of magnitude faster than the reaction with Fe(III) to produce O_2 (reactions R7and R8). Under alkaline conditions, the concentration of $O_2^{•-}$ increases and the production of H_2O_2 through the $O_2^{•-}$ + Fe(II) reaction is much slower than the reaction of $O_2^{•-}$ with Fe(III) to yield O_2 (reactions R9and R10). Therefore, the higher pH is unfavorable for $OH^•$ generation. In addition, the fraction of Fe(III)−oxalate

https://doi.org/10.1021/acs.jpca.2c05919
J. Phys. Chem. A 2023, 127, 250−260

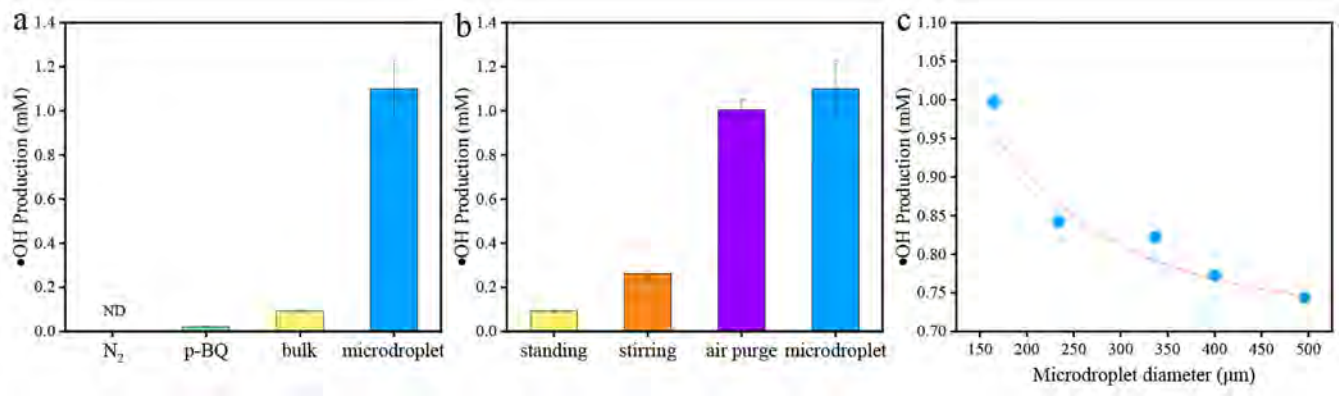

Figure 3. The role of O_2 availability in accelerated hydroxyl radical production. (a) $OH^•$ production by Fe(III)−oxalate photochemistry in aerosol microdroplets and the bulk phase with the addition of an $O_2^{•-}$ scavenger and under a N_2 atmosphere. (b) $OH^•$ production by Fe(III)−oxalate complexes in the bulk phase under different reaction conditions. (c) Concentrations of $OH^•$ in aerosol microdroplets with different sizes. Experimental conditions are as follows: [Fe(III)] = 500 μM, [oxalate] = 3.5 mM, pH 3.5, reaction time of 30 min, [p-BQ] = 10 mM, and agitator speed of 350 rpm min^{-1}.

complexes decreases remarkably as the pH increases, which would also inhibit the generation of $OH^•$.[41] On another hand, as discussed above, the faster photoreactions in microdroplets could result in the rapid consumption of H^+ and increase the pH (reaction R4). In consequence, the $OH^•$ production showed an apparent declining trend in the microdroplets with the increase in the pH and the reaction time. However, the H^+ consumption and pH change in the bulk solution were sluggish as the photoreaction proceeded, leading to the observation of a volcanic plot. Thus, the Fe(III)−oxalate photochemistry for $OH^•$ production would be gradually inhibited by an increase in the pH in an atmospheric environment.

$$HO_2^• + Fe(III) \xrightarrow{-H^+} Fe(II) + O_2 \quad k < 10^4\ M^{-1}\ s^{-1} \tag{R7}$$

$$HO_2^• + Fe(II) \xrightarrow{-H^+} Fe(III) + H_2O_2 \quad k = 1.2 \times 10^6\ M^{-1}\ s^{-1} \tag{R8}$$

$$O_2^{•-} + Fe(III) \rightarrow Fe(II) + O_2 \quad k = 1.5 \times 10^8\ M^{-1}\ s^{-1} \tag{R9}$$

$$O_2^{•-} + Fe(II) \xrightarrow{H^+} Fe(III) + H_2O_2 \quad k = 1.0 \times 10^7\ M^{-1}\ s^{-1} \tag{R10}$$

Furthermore, the influence of the concentration of Fe(III)−oxalate reactants with the same ratio on $OH^•$ production was explored. As shown in Figure 2d, when the concentration of Fe(III)−oxalate chelates increased fivefold, the yield of $OH^•$ in the microdroplet increased from 1.01 to 1.95 mM. However, in the bulk phase, the yield showed an opposite variation trend, namely, the $OH^•$ production decreased from 0.09 to 0.05 mM. The diametrically different variation trend may be due to the fact that in bulk phase $CO_2^{•-}$ mainly interacted with dissolved O_2 at low concentrations of Fe(III)−oxalate complexes, leading to the formation of $OH^•$, whereas at high concentrations of Fe(III)−oxalate $CO_2^{•-}$ would mainly react with Fe(III)−oxalate complexes to form Fe(II) and CO_2 (reaction R11) due to the absence of abundant O_2.[42] However, in microdroplets, the photolysis rate of the Fe(III)−oxalate chelates is fast and the O_2 availability is highly efficient, so the competitive reaction between Fe(III)−oxalate and dissolved O_2 for $CO_2^{•-}$ may not occur even if the concentration of Fe(III)−oxalate chelates is high, which promotes the generation of $OH^•$ as the concentration of the reactions increases. The experimental results show that the generation of $OH^•$ in aerosol microdroplets is not limited by the concentration of Fe(III)−oxalate, showing the distinctiveness of the atmospheric microdroplet environment. Overall, the difference in $OH^•$ production in the microdroplet and the bulk phase further highlights the importance of research in aerosol droplets to fill our knowledge gap in atmospheric photochemistry.

$$[Fe(III)(C_2O_4)_3]^{3-} + CO_2^{•-} \rightarrow [Fe(II)(C_2O_4)_2]^{2-} + CO_2 + C_2O_4^{2-} \tag{R11}$$

3.2. Mechanistic Study for Accelerated $OH^•$ Production. The mechanisms of $OH^•$ production by Fe(III)−oxalate complex photochemistry were studied through radical quenching experiments. To the reaction mixture was added 10 mM *p*-benzoquinone (*p*-BQ) as an $O_2^{•-}$ quencher. As shown in Figure 3a, almost no $OH^•$ was generated in either the microdroplets or the bulk-phase systems, indicating that $O_2^{•-}$ is distinctly important to the production of $OH^•$ (reactions R4−R6). Furthermore, the photoreaction of Fe(III)−oxalate complexes in microdroplets and the bulk phase was carried out under a N_2 atmosphere. Due to the absence of the O_2 supply, no $OH^•$ was detected in microdroplets or the bulk phase (Figure 3a). Thus, it is undoubtable that oxygen is essential to $OH^•$ formation from the Fe(III)−oxalate photo-Fenton processes.

Herein, we speculated that the accelerated $OH^•$ production in microdroplets compared to that in the traditional bulk solution is mainly due to the fact that the microdroplets have large specific surface areas, which are favorable for O_2 accessibility and would provide abundant air−water interfaces with special physicochemical properties. However, for the photoreactions in the bulk solution, the surface area to volume ratio is limited and oxygen mainly exists on the air−water interface. Because of the sluggish diffusivity, it is difficult for O_2 to transfer into the solution, resulting in the incompatibility of the reaction between $CO_2^{•-}$ and O_2 and insufficient $OH^•$ production.[43] To further verify the superiority of microdroplets for O_2 transfer and availability, $OH^•$ production in the bulk phase under magnetic stirring and air purge was conducted for comparison. As shown in Figure 3b, the $OH^•$ concentration

https://doi.org/10.1021/acs.jpca.2c05919
J. Phys. Chem. A 2023, 127, 250−260

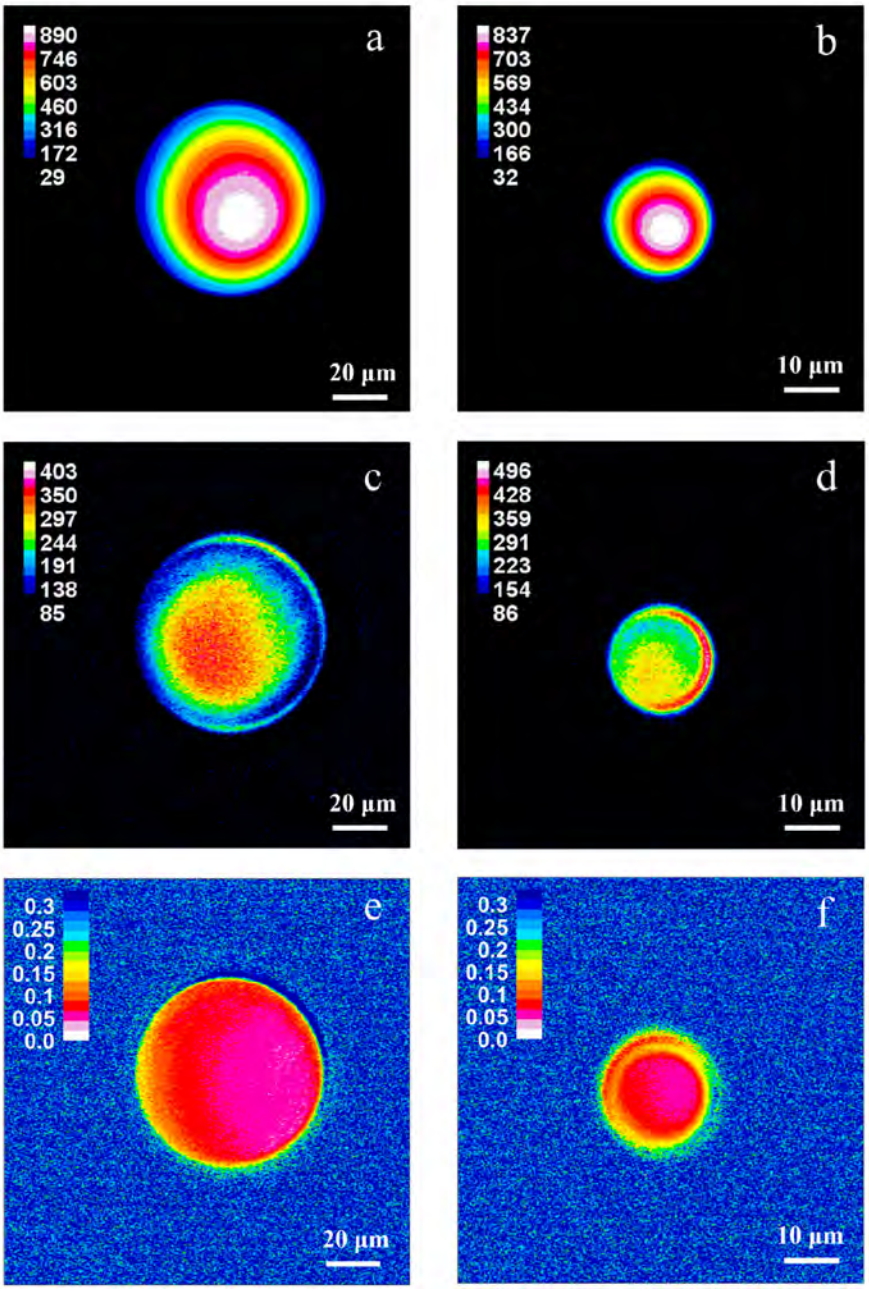

Figure 4. The role of the air−water interface in accelerated hydroxyl radical production. (a and b) Distribution of SRS spectra of ν(O−H) in microdroplets with diameters of 70 and 20 μm, respectively. (c and d) Distribution of SRS spectra of ν(C−C) in microdroplets with diameters of 70 and 20 μm, respectively. (e and f) SRS intensity ratios of ν(C−C) to ν(O−H) in microdroplets with diameters of 70 and 20 μm, respectively. Experimental conditions are as follows: [Fe(III)] = 0.1 M and [oxalate] = 0.5 M.

improved to about 0.25 and 0.97 mM after 30 min of photoreaction under magnetic stirring and air purge, respectively. Even though the $OH^{\bullet}$ production was increased to some extent by stirring and the air purge, the values were still lower than those of microdroplets, demonstrating the considerable ability of aerosol microdroplets to influence gas-involved atmospheric chemistry processes.

Furthermore, $OH^{\bullet}$ production in microdroplets with varying sizes was investigated to explore the influence of aerosol sizes on the atmospheric photochemistry. Microdroplet arrays with a uniform diameter were generated on a superhydrophobic quartz wafer, as shown in Figure 1c. The number of microdroplets with a uniform diameter generated by an inkjet printing device was 625, which corresponded to a 25 × 25 microdroplet array. As displayed in Figure 3c, as the microdroplet diameter decreased from around 495 to 165 μm, it could be found that the $OH^{\bullet}$ production improved significantly, especially for the smaller diameter. The size of actual atmospheric water droplets is in the range of 0.01−100 μm,[20,44] but here we mainly study the photoreactions in microdroplets with diameters larger than 100 μm due to the limitations of the droplet printing device and the operational difficulties of small microdroplets, such as fast volatilization. In spite of this, it is reasonable to extrapolate that the $OH^{\bullet}$ production in authentic atmospheric cloud and fog droplets

https://doi.org/10.1021/acs.jpca.2c05919
J. Phys. Chem. A 2023, 127, 250−260

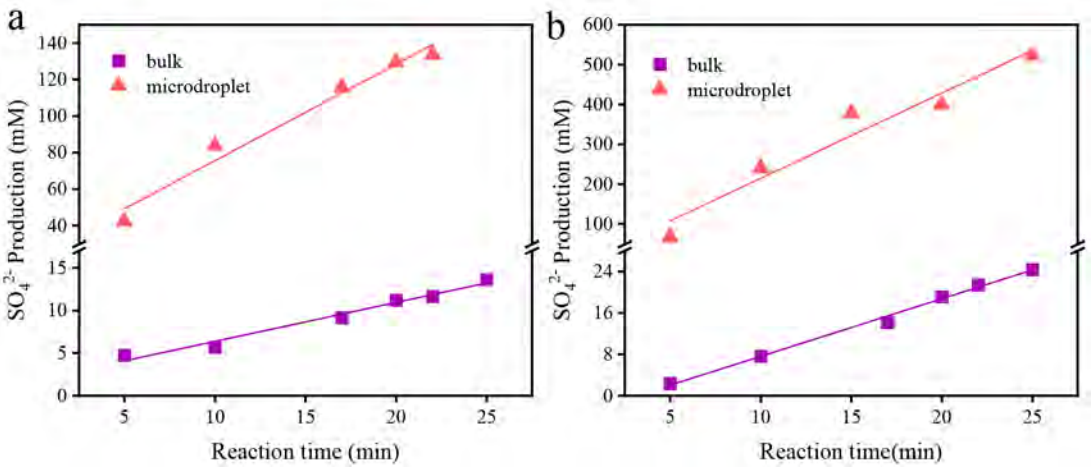

Figure 5. Implication of Fe(III)−oxalate complexes for ambient sulfate formation. (a) Sulfate formation in aerosol microdroplets and the bulk phase under dark conditions. (b) Sulfate formation in microdroplets and the bulk solution under light conditions. Experimental conditions are as follows: [Fe(III)] = 500 μM, [oxalate] = 3.5 mM, pH 3.5, and microdroplet size of 400 μm.

might be more significant because of the smaller size and strengthened droplet physicochemical properties.[24,45]

It has been found that the rates of a variety of redox reactions that occur in microdroplets are significantly accelerated compared to that in the bulk phase reaction because of the enrichment of the reactant concentration near and at the air−water interface.[46] Here, the concentration of Fe(III)−oxalate chelates at the microdroplet air−water interface was explored via stimulated Raman scattering (SRS) microscopy. Figure 4a−d present the distribution of the SRS peak intensity of ν(O−H) and ν(C−C) in microdroplets (Φ = 70 and 20 μm). As shown in Figure 4a and b, the SRS peak intensity of ν(O−H), which is attributed to the O−H bond of a water molecule, weakened from the center to the edge in microdroplet with diameters of 70 and 20 μm because the number of detected molecules decreased at the droplet interfacial region.[47] The same variation trend for ν(C−C) of oxalate molecules was also observed in a microdroplet with a diameter of 70 μm (Figure 4c). However, the surface region in a microdroplet with a diameter of 20 μm showed a comparatively high SRS peak intensity of ν(C−C), probably due to the species concentration increasing at the interface (Figure 4d). Because the spherical shape of the microdroplet could result in the observation of a higher SRS peak intensity at the interface, the internal standard method was adopted to minimize this inference and to qualitatively investigate the species concentration.[48,49] Additionally, the peak intensity ratio of ν(C−C) to ν(O−H) can be regarded as an indicator of the oxalate concentration according to the internal standard method.[50]Figure 4e and f show that the ratio value of ν(C−C) to ν(O−H) in microdroplets was higher near the interfacial region, indicating that the concentration of the oxalate may be enriched at the surface. Previously, Zare et al. reported that concentration enrichment of a molecule generally occurs at the microdroplet surface, as investigated by two-photon fluorescence microscopy, and Allen et al. found significant Fe(III) interfacial enrichment in an aqueous solution using polarized vibrational sum frequency generation (SFG) spectroscopy.[51,52]

Figure S8 whos the effects of the oxalate/Fe(III) molar ratio on $OH^{\bullet}$ production. The results indicated that $OH^{\bullet}$ generation increased with the molar ratio of oxalate/Fe(III), but the enhancement factors between the microdroplet and the bulk phase were not significantly influenced by the oxalate/Fe(III) molar ratio. Because the interface concentration enrichment probably resulted from the intrinsic species surface propensity and a special microdroplet interfacial physicochemical property, the concentration enrichment observed by SRS measurements with the oxalate/Fe(III) molar ratio of 5 was also similar to that in the presence of an oxalate/Fe(III) molar ratio of 7. More importantly, it has been demonstrated that $OH^{\bullet}$ production improved in microdroplets as the concentrations of Fe(III)−oxalate chelates increased, indicating that the interfacial concentration enrichment could make contributions to the $OH^{\bullet}$ production acceleration. Besides, at the microdroplet air−water interface, the accessibility to O_2 is more efficient, and there might be some other special interfacial physicochemical properties such as surface partial solvation and pH alteration, which would also be favorable for the interfacial photochemical reaction and increase $OH^{\bullet}$ production.[46,47] Overall, the Fe(III)−oxalate photochemistry in microdroplets shows a significant $OH^{\bullet}$ production capacity and a strong oxidation potential, which needs much more attention in the research field of atmospheric chemistry.

3.3. SO_2 Oxidation by Fe(III)−oxalate in a Microdroplet. The anthropogenically emitted SO_2 from fossil fuel combustion and industrial facilities is one of the major atmospheric pollutants.[53] SO_2 oxidation in aerosol particles and fog and cloud droplets plays an important role in atmospheric sulfate formation and has a vital impact on acid rain precipitation, haze pollution, human health, and global climate change. SO_2 can be oxidized to sulfate by strong oxidants such as $OH^{\bullet}$, $O_2^{\bullet-}$, dissolved H_2O_2, O_3, and transition-metal ions (TMIs).[54,55] However, most air-quality models currently underestimate the sulfate concentration compared to field observations, which may be because the simulations parameters were obtained from bulk-phase experiments rather than the atmospheric microdroplets.[56,57] Therefore, an understanding of SO_2 conversion in aerosol microdroplets probably can improve the accuracy of model simulations. Oxalate is abundant in atmospheric water droplets and may influence SO_2 oxidation by complexing dissolved iron species.[58] Herein, the effects of Fe(III)−oxalate photochemistry on sulfate formation were studied in microdroplets and compared with the bulk-phase reaction under both light

https://doi.org/10.1021/acs.jpca.2c05919
J. Phys. Chem. A 2023, 127, 250−260

irradiation and dark conditions to verify the necessity considering atmospheric water droplets in atmospheric chemistry process.

As shown in Figure 5, the SO_2 oxidation in microdroplets presented the significantly faster sulfate formation rates than the bulk phase in the presence or absence of light irradiation. Meanwhile, light irradiation promoted SO_2 oxidation. Under dark conditions, the sulfate formation rate in the microdroplet is 11.6× faster than that in the bulk-phase reaction (5.29 mM min^{-1} vs 0.46 mM min^{-1}), while under light irradiation the rate of the microdroplet reaction was 19.1-fold greater than that of the bulk solution (21.41 mM min^{-1} vs 1.11 mM min^{-1}). Furthermore, to better simulate the actual atmospheric environment, the oxidation of a low concentration of 1 ppm SO_2 by Fe(III)−oxalate photochemistry was also studied. As presented in Figure S9, the sulfate production in microdroplets is remarkably higher than that in the bulk phase (120.09 mM vs 2.48 mM), confirming that the SO_2 photooxidation acceleration in aerosol droplets also occurs at low concentrations of SO_2. The dominant sulfate formation mechanisms as presented below (Figure 6).

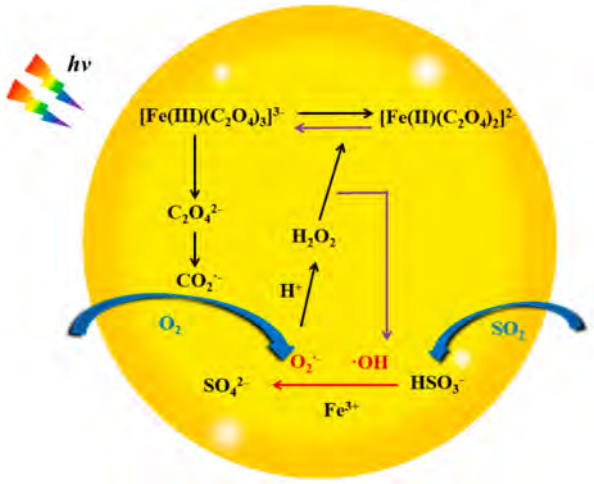

Figure 6. Reaction mechanism of sulfate formation by the photolysis of Fe(III)−oxalate complexes in aerosol microdroplets.

Dissolved Fe(III) in aqueous acidic solutions may appear in the form of Fe(III)−oxalate complexes and Fe(III)−hydroxo complexes. Under dark conditions, $FeOH^{2+}$ could participate in S(IV) oxidation (reaction R12).[59]

$$FeOH^{2+} + HSO_3^- \xrightarrow{O_2} Fe^{2+} + SO_4^{2-} + H_2O \quad (R12)$$

Under light irradiation, Fe(III)−oxalate could generate and release reactive oxygen species (ROS) such as H_2O_2, $O_2^{\bullet-}$, and $OH^{\bullet}$ (reactions R1−R6), leading to enhanced oxidation of dissolved SO_2 compared to that in the dark reactions (reactions R13−R20). Moreover, the photo-oxidation of S(IV) by Fe(III)−oxalate is often accompanied by the redox cycle of Fe(II)/Fe(III) (reaction R21), which might be beneficial to ROS formation and S(IV) oxidation.[58]

$$OH^{\bullet} + HSO_3^- \rightarrow SO_3^{\bullet-} + H_2O \quad (R13)$$

$$HO_2^{\bullet-}/(O_2^{\bullet-} + H^+) + HSO_3^- \rightarrow SO_3^{\bullet-} + H_2O_2 \quad (R14)$$

$$SO_3^{\bullet-} + O_2 \rightarrow SO_5^{\bullet-} \quad (R15)$$

$$SO_5^{\bullet-} + HSO_3^- \rightarrow HSO_4^- + SO_4^{\bullet-} \quad (R16)$$

$$SO_4^{\bullet-} + HSO_3^- \rightarrow SO_4^{2-} + H^+ + SO_3^{\bullet-} \quad (R17)$$

$$SO_4^{\bullet-} + Fe^{2+} \rightarrow Fe^{3+} + SO_4^{2-} \quad (R18)$$

$$SO_4^{\bullet-} + C_2O_4^{2-} \rightarrow SO_4^{2-} + C_2O_4^{\bullet-} \quad (R19)$$

$$H_2O_2 + HSO_3^- \rightarrow SO_4^{2-} + H_2O + H^+ \quad (R20)$$

$$HO_2^{\bullet}/O_2^{\bullet-} + Fe(III) \rightarrow (O_2 + H^+)/O_2 + Fe(II) \quad (R21)$$

Regarding the acceleration of SO_2 oxidation in microdroplets, one of the potential reasons might be the rapid transfer of gaseous molecules (O_2 and SO_2) in microdroplets due to the large specific surface area and limited reaction space. Besides, the air−water interface might also contribute to the acceleration. Hung et al. found that the enhanced uptake of SO_2 on the surfaces of acidic microdroplets was due to interfacial reactions.[60] SO_2 interacts with the hydrated water molecular at the air−water interface via the bonding of sulfur and oxygen. The hydrated SO_2 adducts dissociate into HSO_3^- at the interface and undergo a direct electron transfer with O_2 to yield $SO_3^{\bullet-}$ (reaction R22) because of the lower energy barriers of nanometer-scale length of the interfacial air−water layer. The $SO_3^{\bullet-}$ carrying a negative charge is repelled by the air−water interface and may partly diffuse to the microdroplet core, then initiates a rapid free chain reaction to form sulfate (vide supra).[56,61]

$$HSO_3^- + O_2 \rightarrow SO_3^{\bullet-} + O_2^{\bullet-} + H^+ \quad (R22)$$

Thus, the acceleration of sulfate formation in microdroplets suggests that other atmospheric trace gas conversation processes might also be underestimated, and further studies are needed to estimate and modify the simulation parameters.

4. ATMOSPHERIC IMPLICATIONS

In atmospheric environments, aerosol, cloud, and fog droplets are ubiquitous, and the related chemical reactions might be complex and different from those in bulk solution. Recently, some studies have investigated the atmospheric chemistry processes in micrometer-sized aerosols and droplets, which suggested the particularity of atmospheric chemical reactions in microdroplets.[62,63] Nevertheless, understanding of the complex atmospheric chemistry in authentic water droplets is still very limited. The photochemistry of Fe(III)−oxalate complexes has been shown to be critical in various atmospheric photooxidation processes as a dominant source of $OH^{\bullet}$, such as the oxidative transformations of atmospheric organic and inorganic compounds.[41,64,65] However, little consideration of the special characteristics of atmospheric droplets has been taken into the laboratory experiments and model studies, probably leading to the evident gap between model simulations and field observations. In this work, $OH^{\bullet}$ production by photoreactions of Fe(III)−oxalate complexes in microdroplets and bulk solution were investigated. The $OH^{\bullet}$ production in microdroplets is one order of magnitude higher than in the bulk phase. In addition, we found that the rate of SO_2 oxidation to sulfate was also higher in microdroplets containing Fe(III)−oxalate chelates under both the dark and light irradiation conditions. At present, the acceleration of the

https://doi.org/10.1021/acs.jpca.2c05919
J. Phys. Chem. A 2023, 127, 250−260

photoreactions is mainly attributed to the improved mass transfer and the droplet effect. Our experimental results indicate that, in authentic atmospheric environments, the (photo)chemistry process in cloud and fog droplets and aerosols should receive tremendous research attention and evaluation using microcompartment reactors.

■ ASSOCIATED CONTENT

Supporting Information

The Supporting Information is available free of charge at https://pubs.acs.org/doi/10.1021/acs.jpca.2c05919.

Details of materials and reagents, simulated Raman spectroscopy measurements, effects of Cl^- and the oxalate/Fe(III) molar ratio on $OH^•$ generation, schematic illustration of reaction chamber, water contact angle of superhydrophobic substrate; microdroplet sizes before and after the photoreaction, experimental setup for sulfate formation, calibration curve for *p*-HBA concentration quantitation, enlarged version of $OH^•$ generation in the bulk phase, and sulfate generation in microdroplets and the bulk solution under light conditions (PDF)

■ AUTHOR INFORMATION

Corresponding Author

Liwu Zhang − *Shanghai Key Laboratory of Atmospheric Particle Pollution and Prevention, National Observations and Research Station for Wetland Ecosystems of the Yangtze Estuary, Department of Environmental Science and Engineering, Fudan University, Shanghai 200433, People's Republic of China; Shanghai Institute of Pollution Control and Ecological Security, Shanghai 200092, People's Republic of China;* orcid.org/0000-0002-0765-8660; Email: zhanglw@fudan.edu.cn

Authors

Longqian Wang − *Shanghai Key Laboratory of Atmospheric Particle Pollution and Prevention, National Observations and Research Station for Wetland Ecosystems of the Yangtze Estuary, Department of Environmental Science and Engineering, Fudan University, Shanghai 200433, People's Republic of China; Shanghai Institute of Pollution Control and Ecological Security, Shanghai 200092, People's Republic of China*

Kejian Li − *Shanghai Key Laboratory of Atmospheric Particle Pollution and Prevention, National Observations and Research Station for Wetland Ecosystems of the Yangtze Estuary, Department of Environmental Science and Engineering, Fudan University, Shanghai 200433, People's Republic of China; Shanghai Institute of Pollution Control and Ecological Security, Shanghai 200092, People's Republic of China*

Yangyang Liu − *Shanghai Key Laboratory of Atmospheric Particle Pollution and Prevention, National Observations and Research Station for Wetland Ecosystems of the Yangtze Estuary, Department of Environmental Science and Engineering, Fudan University, Shanghai 200433, People's Republic of China*

Kedong Gong − *Shanghai Key Laboratory of Atmospheric Particle Pollution and Prevention, National Observations and Research Station for Wetland Ecosystems of the Yangtze Estuary, Department of Environmental Science and Engineering, Fudan University, Shanghai 200433, People's Republic of China;* orcid.org/0000-0003-2460-4370

Juan Liu − *Shanghai Key Laboratory of Atmospheric Particle Pollution and Prevention, National Observations and Research Station for Wetland Ecosystems of the Yangtze Estuary, Department of Environmental Science and Engineering, Fudan University, Shanghai 200433, People's Republic of China*

Jianpeng Ao − *State Key Laboratory of Surface Physics and Department of Physics, Fudan University, Shanghai 200433, People's Republic of China*

Qiuyue Ge − *Shanghai Key Laboratory of Atmospheric Particle Pollution and Prevention, National Observations and Research Station for Wetland Ecosystems of the Yangtze Estuary, Department of Environmental Science and Engineering, Fudan University, Shanghai 200433, People's Republic of China*

Wei Wang − *Shanghai Key Laboratory of Atmospheric Particle Pollution and Prevention, National Observations and Research Station for Wetland Ecosystems of the Yangtze Estuary, Department of Environmental Science and Engineering, Fudan University, Shanghai 200433, People's Republic of China*

Minbiao Ji − *State Key Laboratory of Surface Physics and Department of Physics, Fudan University, Shanghai 200433, People's Republic of China*

Complete contact information is available at: https://pubs.acs.org/10.1021/acs.jpca.2c05919

Author Contributions

$^{\nabla}$These authors contributed equally to this work.

Notes

The authors declare no competing financial interest.

■ ACKNOWLEDGMENTS

The authors gratefully acknowledge financial support from National Natural Science Foundation of China (no. 21976030 and no. 22006020), the National Science Foundation of Shanghai (no. 19ZR1471200), and China Postdoctoral Science Foundation (no. 2020M670996).

■ REFERENCES

(1) Tiwari, S.; Kumar, R.; Tunved, P.; Singh, S.; Panicker, A. S. Significant cooling effect on the surface due to soot particles over Brahmaputra River Valley region, India: An impact on regional climate. *Sci. Total Environ.* **2016**, *562*, 504−516.

(2) Desboeufs, K. V.; Losno, R.; Colin, J. L. Factors influencing aerosol solubility during cloud processes. *Atmos. Environ.* **2001**, *35*, 3529−3537.

(3) Pinto, M. J.; Gvirtzman, H.; Gorelick, S. M. Laboratory-scale analysis of aquifer remediation by in-well vapor stripping-2. Modeling results. *J. Contam. Hydrol* **1997**, *29*, 41−58.

(4) Fares, S.; Schnitzhofer, R.; Jiang, X. Y.; Guenther, A.; Hansel, A.; Loreto, F. Observations of diurnal to weekly variations of monoterpene-dominated fluxes of volatile organic compounds from mediterranean forests: implications for regional modeling. *Environ. Sci. Technol.* **2013**, *47*, 11073−11082.

(5) Zhang, R.; Gen, M.; Liang, Z.; Li, Y. J.; Chan, C. K. Photochemical reactions of glyoxal during particulate ammonium nitrate photolysis: brown carbon formation, enhanced glyoxal and phase formation. *Environ. Sci. Technol.* **2022**, *56*, 1605−1614.

(6) Schwarz, J. P.; Spackman, J. R.; Fahey, D. W.; Gao, R. S.; Lohmann, U.; Stier, P.; Watts, L. A.; Thomson, D. S.; Lack, D. A.; Pfister, L.; et al. Coatings and their enhancement of black carbon light

absorption in the tropical atmosphere. *J. Geophys. Res. Atmos.* **2008**, *113*, D03203.
(7) Hegg, D. A.; Clarke, A. D.; Doherty, S. J.; Strom, J. Measurements of black carbon aerosol washout ratio on Svalbard. *Tellus B* **2022**, *63*, 891−900.
(8) Luo, Z.; Min, Y.; Qu, L.; Song, Y.; Hong, Y. Remediation of phenanthrene contaminated soil by ferrous oxalate and its phytotoxicity evaluation. *Chemosphere* **2021**, *265*, 129070.
(9) Yang, C.; Zhou, S. X.; Zhang, C. Y.; Yu, M. Y.; Cao, F.; Zhang, Y. L. Atmospheric Chemistry of Oxalate: Insight into the role of relative humidity and aerosol acidity from high-resolution observation. *J. Geophys. Res. Atmos.* **2022**, *127*, No. e2021JD035364.
(10) Pozdnyakov, I. P.; Kel, O. V.; Plyusnin, V. F.; Grivin, V. P.; Bazhin, N. M. New insight into photochemistry of ferrioxalate. *J. Phys. Chem. A* **2008**, *112*, 8316−8322.
(11) Batista, A. P. S.; Cottrell, B. A.; Nogueira, R. F. P. Photochemical transformation of antibiotics by excitation of Fe-(III)-complexes in aqueous medium. *J. Photochem. Photobiol. A Chem.* **2014**, *274*, 50−56.
(12) Mazellier, P.; Sulzberger, B. Diuron degradation in irradiated, heterogeneous iron/oxalate systems: The rate-determining step. *Environ. Sci. Technol.* **2001**, *35*, 3314−3320.
(13) Mangiante, D. M.; Schaller, R. D.; Zarzycki, P.; Banfield, J. F.; Gilbert, B. Mechanism of ferric oxalate photolysis. *Acs Earth and Space Chem.* **2017**, *1*, 270−276.
(14) Pliego, G.; Zazo, J. A.; Casas, J. A.; Rodriguez, J. J. Fate of iron oxalates in aqueous solution: the role of temperature, iron species and dissolved oxygen. *J. Environ. Chem. Eng.* **2014**, *2*, 2236−2241.
(15) Deguillaume, L.; Leriche, M.; Desboeufs, K.; Mailhot, G.; George, C.; Chaumerliac, N. Transition metals in atmospheric liquid phases: Sources, reactivity, and sensitive parameters. *Chem. Rev.* **2005**, *105*, 3388−3431.
(16) Faust, B. C.; Zepp, R. G. Photochemistry of aqueous iron(III) polycarboxylate complexes-roles in the chemistry of atmospheric and surface waters. *Environ. Sci. Technol.* **1993**, *27*, 2517−2522.
(17) Erokhin, S. E.; Snytnikova, O. A.; Novikov, M. V.; Fedunov, R. G.; Grivin, V. P.; Yanshole, V. V.; Xu, J.; Wu, F.; Plyusnin, V. F.; Pozdnyakov, I. P. Probing reactions between imipramine and hydroxyl radical with the photolysis of iron(III) oxalate: Implications for the indirect photooxidation of tricyclic antidepressants in waters. *J. Photochem. Photobiol. A Chem.* **2022**, *422*, 113559.
(18) Batista, A. P. S.; Nogueira, R. F. P. Parameters affecting sulfonamide photo-Fenton degradation-iron complexation and substituent group. *J. Photochem. Photobiol. A Chem.* **2012**, *232*, 8−13.
(19) Lan, Q.; Liu, H.; Li, F. B.; Zeng, F.; Liu, C. S. Effect of pH on pentachlorophenol degradation in irradiated iron/oxalate systems. *Chem. Eng. J.* **2011**, *168*, 1209−1216.
(20) Herrmann, H.; Schaefer, T.; Tilgner, A.; Styler, S. A.; Weller, C.; Teich, M.; Otto, T. Tropospheric aqueous-phase chemistry: Kinetics, mechanisms, and its coupling to a changing gas phase. *Chem. Rev.* **2015**, *115*, 4259−4334.
(21) Mondal, S.; Acharya, S.; Biswas, R.; Bagchi, B.; Zare, R. N. Enhancement of reaction rate in small-sized droplets: A combined analytical and simulation study. *J. Chem. Phys.* **2018**, *148*, 244704.
(22) Fallah-Araghi, A.; Meguellati, K.; Baret, J. C.; El Harrak, A.; Mangeat, T.; Karplus, M.; Ladame, S.; Marques, C. M.; Griffiths, A. D. Enhanced chemical synthesis at soft interfaces: A universal reaction-adsorption mechanism in microcompartments. *Phys. Rev. Lett.* **2014**, *112*, 028301.
(23) Yan, X.; Bain, R. M.; Cooks, R. G. Organic reactions in microdroplets: Reaction acceleration revealed by mass spectrometry. *Angew. Chem. Int. Ed* **2016**, *55*, 12960−12972.
(24) Lee, J. K.; Walker, K. L.; Han, H. S.; Kang, J.; Prinz, F. B.; Waymouth, R. M.; Nam, H. G.; Zare, R. N. Spontaneous generation of hydrogen peroxide from aqueous microdroplets. *Proc. Natl. Acad. Sci. U.S.A* **2019**, *116*, 19294−19298.
(25) Lee, J. K.; Han, H. S.; Chaikasetsin, S.; Marron, D. P.; Waymouth, R. M.; Prinz, F. B.; Zare, R. N. Condensing water vapor to droplets generates hydrogen peroxide. *Proc. Natl. Acad. Sci. U.S.A* **2020**, *117*, 30934−30941.
(26) Lee, J. K.; Samanta, D.; Nam, H. G.; Zare, R. N. Micron-sized water droplets induce spontaneous reduction. *Proc. Natl. Acad. Sci. U.S.A* **2019**, *141*, 10585−10589.
(27) Nam, I.; Nam, H. G.; Zare, R. N. Abiotic synthesis of purine and pyrimidine ribonucleosides in aqueous microdroplets. *Proc. Natl. Acad. Sci. U.S.A* **2018**, *115*, 36−40.
(28) Nam, I.; Lee, J. K.; Nam, H. G.; Zare, R. N. Abiotic production of sugar phosphates and uridine ribonudeoside in aqueous microdroplets. *Proc. Natl. Acad. Sci. U.S.A* **2017**, *114*, 12396−12400.
(29) Li, K.; Gong, K.; Liu, J.; Ohnoutek, L.; Ao, J.; Liu, Y.; Chen, X.; Xu, G.; Ruan, X.; Cheng, H.; et al. Significantly accelerated photochemical and photocatalytic reactions in microdroplets. *Cell Rep. Phys. Sci.* **2022**, *3*, 100917.
(30) Wang, Y.; Brigante, M.; Mailhot, G.; Talaga, D.; Wu, Y. L.; Dong, W. B.; Sobanska, S. Toward a better understanding of ferric-oxalate complex photolysis: The role of the aqueous/air interface of droplet. *Chemosphere* **2022**, *289*, 133127.
(31) Thomas, D. A.; Coggon, M. M.; Lignell, H.; Schilling, K. A.; Zhang, X.; Schwantes, R. H.; Flagan, R. C.; Seinfeld, J. H.; Beauchamp, J. L. Real-time studies of iron oxalate-mediated oxidation of glycolaldehyde as a model for photochemical aging of aqueous tropospheric Aerosols. *Environ. Sci. Technol.* **2016**, *50*, 12241−12249.
(32) Joo, S. H.; Feitz, A. J.; Sedlak, D. L.; Waite, T. D. Quantification of the oxidizing capacity of nanoparticulate zero-valent iron. *Environ. Sci. Technol.* **2005**, *39*, 1263−1268.
(33) Zhang, P.; Yuan, S. H.; Liao, P. Mechanisms of hydroxyl radical production from abiotic oxidation of pyrite under acidic conditions. *Geochim. Cosmochim. Acta* **2016**, *172*, 444−457.
(34) Li, K.; Wang, L.; Liu, J.; Gong, K.; Wang, W.; Ge, Q.; Liu, Y.; Zhang, L. A protocol to study microdroplet photoreaction at an individual droplet level using *in situ* micro-Raman spectroscopy. *Star. Protoc* **2022**, *3*, 101704.
(35) Xing, D.; Meng, Y. F.; Yuan, X.; Jin, S. H.; Song, X. W.; Zare, R. N.; Zhang, X. X. Capture of Hydroxyl Radicals by Hydronium Cations in Water Microdroplets. *Angew. Chem. Int. Ed* **2022**, *61*, No. e202207587.
(36) Zhou, X.; Mopper, K. Determination of photochemically produced hydroxyl radicals in seawater and freshwater. *Mar. Chem.* **1990**, *30*, 71−88.
(37) Wang, T.; Liu, Y. Y.; Deng, Y.; Cheng, H. Y.; Yang, Y.; Li, K. J.; Fang, X. Z.; Zhang, L. W. Irradiation intensity dependent heterogeneous formation of sulfate and dissolution of ZnO nanoparticles. *Environ. Sci.: Nano* **2020**, *7*, 327−338.
(38) Chen, L.; Feng, X. J. Enhanced catalytic reaction at an air-liquid-solid triphase interface. *Chem. Sci.* **2020**, *11*, 3124−3131.
(39) Liu, Z.; Sheng, X.; Wang, D. D.; Feng, X. J. Efficient hydrogen peroxide generation utilizing photocatalytic oxygen reduction at a triphase interface. *iScience* **2019**, *17*, 67−73.
(40) Huang, D.; Wang, J. Z.; Xia, H. L.; Zhang, Y.; Bao, F. X.; Li, M.; Chen, C. C.; Zhao, J. C. Enhanced photochemical volatile organic compounds release from fatty acids by surface-enriched Fe(III). *Environ. Sci. Technol.* **2020**, *54*, 13448−13457.
(41) Zuo, Y. G.; Hoigne, J. Formation of hydrogen-peroxide and depletion of oxalic-acid in atmospheric water by photolysis of iron(III)-oxalato complexes. *Environ. Sci. Technol.* **1992**, *26*, 1014−1022.
(42) Jeong, J. S.; Yoon, J. Y. Dual roles of $CO_2^{\cdot-}$ for degrading synthetic organic chemicals in the photo/ferrioxalate system. *Wat. Res.* **2004**, *38*, 3531−3540.
(43) Yu, G. S.; Wang, N. Gas-Liquid-Solid interface enhanced photocatalytic reaction in a microfluidic reactor for water treatment. *Appl. Catal. A Gen* **2020**, *591*, 117410.
(44) Pöschl, U. Atmospheric aerosols: Composition, transformation, climate and health effects. *Angew. Chem. Int. Ed* **2005**, *44*, 7520−7540.
(45) Chamberlayne, C. F.; Zare, R. N. Simple model for the electric field and spatial distribution of ions in a microdroplet. *J. Chem. Phys.* **2020**, *152*, 184702.

(46) Anglada, J. M.; Martins-Costa, M. T. C.; Francisco, J. S.; Ruiz-Lopez, M. F. Photoinduced oxidation reactions at the air-water interface. *J. Am. Chem. Soc.* **2020**, *142*, 16140−16155.
(47) Wei, H.; Vejerano, E. P.; Leng, W.; Huang, Q.; Willner, M. R.; Marr, L. C.; Vikesland, P. J. Aerosol microdroplets exhibit a stable pH gradient. *Proc. Natl. Acad. Sci. U. S. A* **2018**, *115*, 7272−7277.
(48) Pelletier, M. J. Quantitative Analysis Using Raman Spectrometry. *Appl. Spectrosc.* **2003**, *57*, 20A.
(49) Wang, P.; Li, J. J.; Wang, P.; Hu, C. R.; Zhang, D. L.; Sturek, M.; Cheng, J. X. Label-Free Quantitative Imaging of Cholesterol in Intact Tissues by Hyperspectral Stimulated Raman Scattering Microscopy. *Angew. Chem. Int. Ed* **2013**, *52*, 13042−13046.
(50) Aarnoutse, P. J.; Westerhuis, J. A. Quantitative Raman reaction monitoring using the solvent as internal standard. *Anal. Chem.* **2005**, *77*, 1228−1236.
(51) Lin, L.; Husek, J.; Biswas, S.; Baumler, S. M.; Adel, T.; Ng, K. C.; Baker, L. R.; Allen, H. C. Iron(III) Speciation Observed at Aqueous and Glycerol Surfaces: Vibrational Sum Frequency and X-Ray. *J. Am. Chem. Soc.* **2019**, *141*, 13525−13535.
(52) Xiong, H. Q.; Lee, J. K.; Zare, R. N.; Min, W. Strong Concentration Enhancement of Molecules at the Interface of Aqueous Microdroplets. *J. Phys. Chem. B* **2020**, *124*, 9938−9944.
(53) Buchard, V.; da Silva, A. M.; Colarco, P.; Krotkov, N.; Dickerson, R. R.; Stehr, J. W.; Mount, G.; Spinei, E.; Arkinson, H. L.; He, H. Evaluation of GEOS-5 sulfur dioxide simulations during the Frostburg, MD 2010 field campaign. *Atmos. Chem. Phys.* **2014**, *14*, 1929−1941.
(54) Tan, J. H.; Duan, J. C.; Zhen, N. J.; He, K. B.; Hao, J. M. Chemical characteristics and source of size-fractionated atmospheric particle in haze episode in Beijing. *Atmos. Res.* **2016**, *167*, 24−33.
(55) Huang, L. B.; Cochran, R. E.; Coddens, E. M.; Grassian, V. H. Formation of organosulfur compounds through transition metal ion-catalyzed aqueous phase reactions. *Environ. Sci. Technol. Let* **2018**, *5*, 315−321.
(56) Chen, Z.; Liu, P.; Wang, W.; Cao, X.; Liu, Y. X.; Zhang, Y. H.; Ge, M. Rapid sulfate formation via uncatalyzed autoxidation of sulfur dioxide in aerosol microdroplets. *Environ. Sci. Technol.* **2022**, *56*, 7637−7646.
(57) Wang, W.; Liu, M.; Wang, T.; Song, Y.; Zhou, L.; Cao, J.; Hu, J.; Tang, G.; Chen, Z.; Li, Z. J. Sulfate formation is dominated by manganese-catalyzed oxidation of SO_2 on aerosol surfaces during haze events. *Nat. Commun.* **2021**, *12*, 1993.
(58) Zuo, Y.; Zhan, J. Effects of oxalate on Fe-catalyzed photooxidation of dissolved sulfur dioxide in atmospheric water. *Atmos. Environ.* **2005**, *39*, 27−37.
(59) Ge, W. D.; Liu, J. F.; Yi, K.; Xu, J. Y.; Zhang, Y. Z.; Hu, X. R.; Ma, J. M.; Wang, X. J.; Wan, Y.; Hu, J. Y.; et al. Influence of atmospheric in-cloud aqueous-phase chemistry on the global simulation of SO_2 in CESM2. *Atmos. Chem. Phys.* **2021**, *21*, 16093−16120.
(60) Hung, H.-M.; Hsu, M.-N.; Hoffmann, M. R. Quantification of SO_2 oxidation on interfacial surfaces of acidic micro-droplets: Implication for ambient sulfate formation. *Environ. Sci. Technol.* **2018**, *52*, 9079−9086.
(61) Hung, H.-M.; Hoffmann, M. R. Oxidation of gas-phase SO_2 on the surfaces of acidic microdroplets: Implications for sulfate and sulfate radical anion formation in the atmospheric liquid phase. *Environ. Sci. Technol.* **2015**, *49*, 13768−13776.
(62) Franco, B.; Blumenstock, T.; Cho, C.; Clarisse, L.; Clerbaux, C.; Coheur, P. F.; De Maziere, M.; De Smedt, I.; Dorn, H. P.; Emmerichs, T.; et al. et al. Ubiquitous atmospheric production of organic acids mediated by cloud droplets. *Nature* **2021**, *593*, 233−237.
(63) de Gouw, J.; Farmer, D. Cloud droplets aid the production of formic acid in the atmosphere. *Nature* **2021**, *593*, 198−199.
(64) Pang, H.; Zhang, Q.; Wang, H.; Cai, D.; Ma, Y.; Li, L.; Li, K.; Lu, X.; Chen, H.; Yang, X.; et al. Photochemical aging of guaiacol by Fe(III)−Oxalate complexes in atmospheric aqueous phase. *Environ. Sci. Technol.* **2019**, *53*, 127−136.
(65) Wang, Y.; Zhao, J.; Liu, H.; Li, Y.; Dong, W.; Wu, Y. Photooxidation of methacrolein in Fe(III)-oxalate aqueous system and its atmospheric implication. *Adv. Atmos. Sci.* **2021**, *38*, 1252−1263.

Recommended by ACS

Estimation of Mineral Accessible Surface Area from Mineral Abundance and Clay Content
Fanqi Qin, Lauren E. Beckingham, *et al.*
JANUARY 12, 2023
ACS EARTH AND SPACE CHEMISTRY
READ

Constraining the Effect of Surfactants on the Hygroscopic Growth of Model Sea Spray Aerosol Particles
Rachel L. Bramblett and Amanda A. Frossard
NOVEMBER 10, 2022
THE JOURNAL OF PHYSICAL CHEMISTRY A
READ

A Kinetic Model for Predicting Trace Gas Uptake and Reaction
Kevin R. Wilson, Megan D. Willis, *et al.*
SEPTEMBER 28, 2022
THE JOURNAL OF PHYSICAL CHEMISTRY A
READ

Airborne Microbial Aerosol Detection by Combining Single Particle Mass Spectrometry and a Fluorescent Aerosol Particle Sizer
Han Lun Lu, Xuan Li, *et al.*
DECEMBER 15, 2022
ANALYTICAL CHEMISTRY
READ

Get More Suggestions >

https://doi.org/10.1021/acs.jpca.2c05919
J. Phys. Chem. A 2023, 127, 250−260